Materials Advances

ROYAL SOCIETY OF CHEMISTRY

PAPER

View Article Online
View Journal | View Issue

Cite this: *Mater. Adv.*, 2026, 7, 5171

$Pr_{0.7}Ca_{0.3}Mn_{0.8}Cr_{0.2}O_3$ as a promising candidate for sensor and thermistor applications: investigation of TCR, SF, β, and α parameters

R. Hanen, Y. Moualhi * and H. Rahmouni

Received 20th February 2026,
Accepted 17th April 2026

DOI: 10.1039/d6ma00250a

rsc.li/materials-advances

Motivated by potential sensor and thermistor applications, a detailed study of the electrical behavior of $Pr_{0.7}Ca_{0.3}Mn_{0.8}Cr_{0.2}O_3$ (PCMCO) ceramic was carried out. Additionally, to gain deeper insight into the charge transport mechanisms in the studied material, different theoretical conduction models were employed. Indeed, DC-conductance measurements confirm the semiconducting behavior over the investigated temperature range. According to Holstein's theory, the charge transport mechanism in $Pr_{0.7}Ca_{0.3}Mn_{0.8}Cr_{0.2}O_3$ at elevated temperatures is primarily controlled by non-adiabatic small polaron hopping (NSPH). At low temperatures, the variable range hopping (VRH) mechanism becomes dominant. Furthermore, the temperature coefficient of resistance (TCR) was evaluated to characterize the material's thermo-resistive behavior, highlighting its potential for application in technological devices. It was found that the studied material exhibits a high TCR, reaching $-20.72\%\ K^{-1}$ at 100 K, indicating its promise for use in sensor devices. By determining key thermistor parameters such as the stability factor (SF), sensitivity parameter (β), and sensitivity factor (α), $Pr_{0.7}Ca_{0.3}Mn_{0.8}Cr_{0.2}O_3$ is considered a promising candidate for thermistor applications. The frequency-dependent conductance spectrum, observed between 80 K and 280 K, is well described by Jonscher's power law, revealing both hopping and tunneling transport processes.

1. Introduction

Manganite systems with the general formula $AMnO_3$, particularly those doped with rare-earth elements have attracted extensive scientific interest due to their distinctive structural, electrical and magnetic properties.[1–9] These properties render them promising candidates for various technological applications. Notably, owing to their favorable mixed ionic–electronic conductivity and high thermal stability, manganites have demonstrated significant potential for solid oxide fuel cells (SOFCs).[10,11] These materials are also used in spintronic devices and magnetic sensors due to their pronounced magnetoresistive behavior and transport anisotropy arising from lattice distortions.[11–15] Furthermore, manganites are deemed suitable for use in photovoltaic devices as well as optoelectronic applications, as reported in previous studies[16,17] and in our prior work.[4] Therefore, several research teams have extensively investigated the physical properties of these systems. Among the extensively studied manganite systems, praseodymium-based manganites have attracted significant attention due to their diverse physical properties. The properties of these materials are strongly influenced by the complex interplay between their spin, charge orbital and magnetic degrees of freedom.[9,18,19] Accordingly, the improvement of their physical properties is principally controlled by the modification of several factors such as the nature of the dopant element, its concentration, and appropriate substitution at the A site, the Mn site, or simultaneously at both the A and Mn sites.[8,20–25] In recent years, several studies have extensively explored the effects of doping at the Mn site in manganite materials.[2,4,7,8,26–29] Such an approach offers an effective strategy of tuning their structural, electrical, and magnetic properties by directly altering the Mn^{3+}/Mn^{4+} ratio. Additionally, it influences the double-exchange (DE) interactions and the dynamics of polarons.[2] Furthermore, Mn-site substitution can induce significant changes in the relative cooling power (RCP) and the magnetoresistance response; therefore, modification of the transport properties of these materials.[28,30–33] In this regard, substituting Mn with other transition metals possessing different electronic configurations results in significant changes to the electronic structures of both Mn and the substituting elements. As a result, the type of dopant element and the microstructure play a major role in governing the conduction mechanisms, the dynamics of the charge carriers, and thermally activated transport phenomena. It equally influences the

Laboratoire de Recherche Matériaux Avancés et Nanotechnologies (LRMAN), Institut Supérieur des Sciences Appliquées et de Technologie de Kasserine, Université de Kairouan, BP 471, 1200 Kasserine, Tunisia. E-mail: moualhiyoussef7@gmail.com

colossal magnetoresistance, which in turn modifies the overall physical properties of manganite systems.[1] Among the various dopant elements at the Mn site, doping by chromium (Cr^{3+}) ions is one of the most intensively studied substitutions by many research groups.[31,32,34–36] Its electronic configuration is similar to that of the Mn^{3+} ion; however, it is devoid of an itinerant (e_g) electron.[37] As a result, Jahn–Teller distortions are effectively suppressed, leading to significant alterations in the Mn–O–Mn super-exchange channels.[37] In ref. 2, the authors reported that the introduction of Cr element at the Mn site might disturb long-range double-exchange conduction. Accordingly, it strengthens electron–phonon coupling and favors the formation of small polarons. According to the reported results in ref. 38, chromium ion act as effective dopants for inducing a metal–insulator transition in charge-ordering (CO) manganite compounds, leading to an enhancement of the colossal magnetoresistance effect. It is worth noting that the level of Cr substitution plays a crucial role in determining the transport properties of Pr–Ca manganites. While low Cr concentrations generally induce moderate perturbations in the Mn^{3+}/Mn^{4+} network, higher substitution levels can lead to significant modifications of the electronic structure and charge transport mechanisms. In particular, a Cr content as high as 20% is expected to strongly disrupt the double-exchange interaction and enhance carrier localization effects. This can result in a qualitative transition from partially delocalized transport to a regime dominated by hopping conduction processes. In this context, the composition $Pr_{0.7}Ca_{0.3}Mn_{0.8}Cr_{0.2}O_3$ offers an interesting platform to explore the interplay between strong localization, hopping dynamics, and thermo-resistive performance. However, despite its potential, such a high Cr substitution level has not been sufficiently investigated in terms of its combined impact on electrical transport and thermistor-related properties, which motivates the present study. To understand the dynamics of charge carriers within several oxides, numerous theoretical approaches have been developed to explain the electrical transport properties of manganites in both DC and AC regimes.[39–46] In the DC regime, the small polaron hopping (SPH), and the variable range hopping (VRH) models are principally used to explain the origin of the semiconducting behavior observed in various classes of oxides. At elevated temperatures, the adiabatic and the non-adiabatic models developed within Holstein's theory have been extensively used to analyze the electrical behavior of a wide range of materials.[47] Nevertheless, in the AC regime, the high-frequency conductance spectra typically exhibit a power-law behavior. Accordingly, the transport properties in this region arise from the combined contributions of both hopping and tunneling conduction mechanisms.[44–46,48] Tang *et al.*[49] and Pi *et al.*[50] have found that, in perovskite systems, the solubility of certain dopants is limited to $x = 0.2$. Thus, a large Cr content was deliberately chosen to enhance the electrical properties of $Pr_{0.7}Ca_{0.3}MnO_3$ manganite while remaining within the permissible concentration limit in perovskite systems. This enhancement with higher Cr amount is particularly relevant for the negative temperature coefficient (NTC) behavior and the temperature coefficient of resistance (TCR) in praseodymium-based manganites. In contrast to our previous studies on Cr-doped Pr–Ca manganites, which mainly focused on fundamental transport behavior, the present work aims to establish a direct link between charge transport mechanisms and thermistor functionality. Particular attention is devoted to the composition $Pr_{0.7}Ca_{0.3}Mn_{0.8}Cr_{0.2}O_3$, for which a comprehensive investigation of both DC and AC electrical properties is performed in conjunction with a detailed evaluation of key thermistor parameters, including the temperature coefficient of resistance (TCR), sensitivity parameter (β), sensitivity factor (α), and stability factor (SF). Notably, the material exhibits an enhanced TCR in the low-temperature regime, highlighting its potential for sensitive thermal detection. By correlating the dominant conduction mechanisms namely, non-adiabatic small polaron hopping at high temperatures and variable range hopping at low temperatures with device-relevant performance metrics, this study provides a more application-oriented perspective that goes beyond conventional transport analysis.

2. Experimental details

Manganite-based oxide systems can generally be prepared using a variety of preparation techniques, each providing specific advantages depending on the desired material properties. In the present investigation, the solid-state reaction method was employed to synthesize the $Pr_{0.7}Ca_{0.3}Mn_{0.8}Cr_{0.2}O_3$ compound due to its simplicity and suitability for large-scale production. Additionally, high-purity precursors Pr_6O_{11}, $CaCO_3$, Cr_2O_3, and Mn_2O_3 were used to prepare the studied manganite, mixed in the desired stoichiometric ratios according to the following chemical reaction:

$$0.7/6Pr_6O_{11} + 0.3CaCO_3 + 0.4Mn_2O_3 + 0.1Cr_2O_3 \rightarrow Pr_{0.7}Ca_{0.3}Mn_{0.8}Cr_{0.2}O_3 + 0.3CO_2 + \delta O_2 \quad (1)$$

The resulting powders are subsequently pressed into pellets. They are then sintered sequentially at 800, 1000, 1100, and 1300 °C for 24 h per cycle.[30] Intermediate regrinding and repelletizing are performed to ensure privileged crystallization.[30] The obtained compound is finally cooled from the high sintering temperature to room temperature following the cooling inertia of the furnace ($\sim$8 h). For structural characterization, the crystal structure for $Pr_{0.7}Ca_{0.3}Mn_{0.8}Cr_{0.2}O_3$ sample was performed at room temperature by X-ray powder diffraction (XRD) with Cu Kα radiation. As reported in ref. 30, this manganite forms a single phase without detectable impurities, crystallizing an orthorhombic structure with the Pnma space group. For the electrical characterization, all the achieved electrical measurements are affected using impedance spectroscopy technique over a wide frequency range [40–4 $\times$ 10^6 Hz]. A thin layer of silver is deposited on the two opposite faces of the pellet form a plate capacitor configuration, allowing for electrical measurements. After that, the investigated $Pr_{0.7}Ca_{0.3}Mn_{0.8}Cr_{0.2}O_3$ is installed in Janis VPF-800 cryostat to control the temperature between 80 K and 300 K. Under vacuum and in

darkness, measurements are taken using an Agilent 4294 analyzer with a 20 mV excitation signal.

3. Results and discussion

3.1 DC-conductance analysis

The temperature dependence of the DC electrical conductance (G_{dc}) of $Pr_{0.7}Ca_{0.3}Mn_{0.8}Cr_{0.2}O_3$ manganite is shown in Fig. 1(a). Over the investigated temperature region (from T = 80 K to T = 300 K), G_{dc} is found to increase monotonically with increasing temperature indicating the semiconducting behavior of the studied system. According to the results reported in ref. 17, such experimental observation can be associated with the localization of charge carriers, which arises from the enhancement of electron–phonon interaction coupled with lattice distortions. Additionally, in $Pr_{0.7}Ca_{0.3}MnO_3$ manganite structure, the electrical transport properties are principally controlled by the double-exchange (DE) mechanism between Mn^{3+}cations and Mn^{4+} cations *via* oxygen anions.[51] This process facilitates the movement of electrons from one site to another. In our system, substituting chromium at the Mn site disturbs the Mn conduction pathways. This effect suppresses the DE interaction leading to a reduction in charge carrier mobility as commonly reported for Cr-substituted manganites.[52] As a result, an enhancement in carrier localization, accompanied by thermally activated transport, results in an increase in G_{dc} with temperature. On the other hand, the electrical transport properties of the manganite are strongly influenced by the microstructure of the material. It has been reported that the introduction of Cr at the Mn site primarily affects the grain boundaries, which play an important role in controlling the movement of the charge carriers.[2] These grain boundaries, which are more resistive than the grain interiors, act as barriers that hinder the movement of charge carriers, thereby enhancing their localization. To overcome these barriers, the charge carriers need sufficient thermal energy. Therefore, the electrical conductance of $Pr_{0.7}Ca_{0.3}Mn_{0.8}Cr_{0.2}O_3$ increases with increasing temperature, which is a characteristic feature of semiconducting behavior. In the DC conductance regime, the observed semiconducting behavior is principally related to the contribution of different conduction processes. The small polaron hopping (SPH) and the variable range hopping (VRH) models are the two mechanisms that can be used to describe the transport properties of $Pr_{0.7}Ca_{0.3}Mn_{0.8}Cr_{0.2}O_3$ system. At high temperatures and beyond half of the Debye temperature ($\theta_D/2$), the electrical conductance evolution is related to the thermal activation of the SPH mechanism. Therefore, the electrical conduction in this process occurs between nearest-neighbor sites. Additionally, the temperature at which the high-temperature linear region begins to deviate from linear behavior is commonly associated with $\theta_D/2$, where θ_D denotes as the Debye temperature.[53] In the literature,[54–56] the SPH mechanism is explained in terms of the adiabatic SPH (ASPH) and the non-adiabatic SPH (NSPH) models. The latter is mainly introduced to justify the transport properties at elevated temperatures. According to these models,

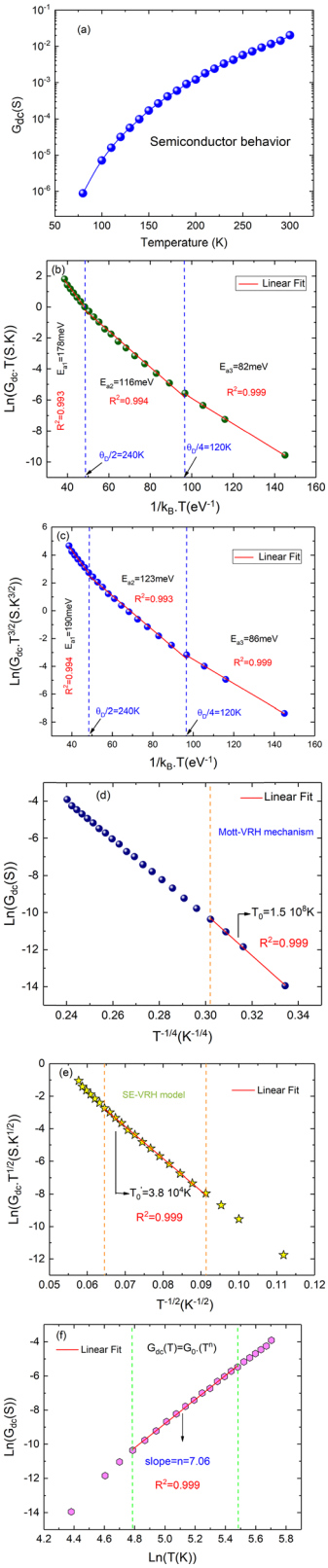

Fig. 1 (a)–(f) Temperature dependence of the DC-conductance (G_{dc}) for $Pr_{0.7}Ca_{0.3}Mn_{0.8}Cr_{0.2}O_3$ compound (a). Evolution of $\ln(G_{dc}\cdot T)$ (b) and $\ln(G_{dc}\cdot T^{3/2})$ (c) against $1/k_BT$. Variation of $\ln(G_{dc})$ *versus* $T^{-1/4}$ (d). Variation of $\ln(G_{dc}\cdot T^{1/2})$ against $T^{-1/2}$ (e). Variation of $\ln(G_{dc})$ as a function of $\ln(T)$ (f).

the temperature dependence of the dc-conductance is given by eqn (2) and (3), respectively, for ASPH and NSPH processes as follows:[47]

$$G_{dc} \cdot T = A \exp\left(\frac{-E_a}{k_B T}\right) \quad (2)$$

$$G_{dc} \cdot T^{3/2} = A \exp\left(\frac{-E_a}{k_B T}\right) \quad (3)$$

where E_a is the activation energy, required for the displacement of charge carriers between two states. It can be expressed according to the following relation:[57]

$$E_a = E_H + E_D/2 \quad \text{for } T > \theta_D/2 \quad (4)$$

$$E_a = E_D \quad \text{for } T < \theta_D/4 \quad (5)$$

E_H, and E_D represent respectively the polaron hopping and disorder energy. The appearance of disorder energy arises from the local arrangement of the ions variation.[39,40,42,43] For ASPH and NSPH models, the variation of $\ln(G_{dc}\cdot T)$ and $\ln(G_{dc}\cdot T^{3/2})$ as a function of the inverse temperature for $Pr_{0.7}Ca_{0.3}Mn_{0.8}Cr_{0.2}O_3$ compound are shown in Fig. 1(b) and (c). At high temperatures and for $T > \theta_D/2$, each conductance curve exhibits a linear behavior, that confirms the thermally activation of the adiabatic SPH (ASPH) or the non-adiabatic SPH (NSPH) mechanisms. For the investigated $Pr_{0.7}Ca_{0.3}Mn_{0.8}Cr_{0.2}O_3$, the deduced Debye temperature is θ_D = 480 K. Based on the Holstein's theory,[54,55] the dominant mechanism of the SPH process can be defined by comparing the ratio between both polaron bandwidth J as well as the critical polaron energy bandwidth Φ. If $\frac{J}{\Phi} > 1$, the transport properties of the investigated material at high temperatures are dominated by the ASPH model. Conversely, for the NSPH model, $\frac{J}{\Phi} < 1$. In this case, the parameters J and Φ are deduced using the following expressions:[54,55]

$$J = 0.67 h\vartheta_{ph}\left(\frac{T}{\theta_D}\right)^{1/4} \quad (6)$$

$$\Phi = \left(\frac{2k_B T E_a}{\pi}\right)^{\frac{1}{4}}\left(\frac{h\vartheta_{ph}}{\pi}\right)^{\frac{1}{2}} \quad (7)$$

The parameters h and k_B correspond respectively to the Planck and Boltzmann constants (h = 4.14375 × 10^{-15} eV s and k_B = 8.617333 × 10^{-5} eV K^{-1}). ϑ_{ph} is the optical phonon frequency as evaluated from the expression:[58] $h\vartheta_{ph} = k_B\theta_D$. From the linear fits of the ASPH and NSPH models, the extracted electrical parameters values are summarized in Table 1. It is found that the calculated values of $\frac{J}{\Phi}$ are 0.92 and 0.90 for the ASPH and NSPH models, respectively. In this case, the calculated $\frac{J}{\Phi}$ ratio is less than 1 after the application of both models, indicating that the NSPH is the most adequate model for describing the observed high-temperature behavior of $Pr_{0.7}Ca_{0.3}Mn_{0.8}Cr_{0.2}O_3$. Accordingly, the temperature dependence of dc-conductance obeys the eqn (3). To get insight into the type of electron–phonon interaction, it is useful to calculate the value of the coupling polaron (γ_p) using the formula:[59] $\gamma_p = \frac{2E_H}{h\vartheta_{ph}}$. Based on the found results in Table 1, and for the NSPH process γ_p is equal to 7.16. As reported by Millis[60] a powerful electron–phonon interaction takes place when $\gamma_p > 4$, whereas a weak electron–phonon interaction dominates when $\gamma_p < 4$. As a result, the coupling polaron γ_p plays a crucial role in determining the main properties of the material. Consequently, the γ_p value is an effective parameter for characterizing the electron–phonon interaction. In our investigation, the obtained value of γ_p clearly satisfies this condition (γ_p = 7.16 > 4). Such result confirms the appearance of strong electron–phonon interaction in $Pr_{0.7}Ca_{0.3}Mn_{0.8}Cr_{0.2}O_3$. The same behavior is recently observed in other manganite systems like $La_{0.8}Ca_{0.2}Mn_{0.5}Ni_{0.5}O_3$ oxide.[61] To affirm again this strong interaction in the studied compound, we can evaluate the value of $\frac{m_p}{m^*}$ according to the formula:[58]

$$\frac{m_p}{m^*} = \left(\frac{h^2}{m^* 8\pi^2 J R^2}\right)\exp(\gamma_p) = \exp(\gamma_p) \quad (8)$$

where m_p, and m^* are respectively the polaron mass and the rigid lattice effective mass. It is found that the $\frac{m_p}{m^*}$ value from the NSPH approach is $\frac{m_p}{m^*} = 1286$. Such a large value further indicates the strong electron–phonon interaction.

Fig. 1(d) shows the variation of $\ln(G_{dc})$ *versus* $T^{-1/4}$. Below θ_D/4, the observed linearity of the plotted curve indicates that the charge transport in the studied compound is governed by the Mott-VRH mechanism. Hence, the temperature dependence of G_{dc} is expressed by the following equation:[62,63]

$$G_{dc}(T) = G_0 \exp\left(\frac{-T_0}{T}\right)^{1/4} \quad (9)$$

G_0 is the pre-exponential factor. T_0 is a characteristic temperature, which was used to determine the density of states value ($N(E_F)$) at the Fermi level. Such a parameter was obtained using the relation cited below:

$$N(E_F) = \frac{16\alpha^3}{k_B T_0} \quad (10)$$

Here α represents the inverse localization length (*i.e.*, the spatial extent of the localized wave function). From the linear Fit of Fig. 1(d), the experimental value of T_0 was deduced and found to be 1.5 × 10^8 K. This value is in good agreement with predictions of Mott's assumption,[39,40,42,43] which mentioned a characteristic T_0 in the order of 10^8 K. Based on the expression

Table 1 The deduced parameters from the adiabatic and the non-adiabatic models for $Pr_{0.7}Ca_{0.3}Mn_{0.8}Cr_{0.2}O_3$

	E_{a1} (eV)	E_H (eV)	E_D (eV)	θ_D (K)	ϑ_{ph} (Hz)	$\frac{J}{\Phi}$	γ_p
ASPH	0.178	0.137	0.082	480	0.99 × 10^{13}	0.92	6.67
NSPH	0.190	0.147	0.086	480	0.99 × 10^{13}	0.90	7.16

(10), the value of $N(E_F)$ was calculated, $N(E_F) = 1.23 \times 10^{24}$ eV^{-1} cm^{-3} for $\alpha^{-1} = 10$ Å.[64] At temperatures surpassing $\theta_D/4$, the increase in temperature leads to an improvement in the density of mobile charge carriers, inducing a strong electron-lattice coupling.[39,40,42,43] Therefore, the contribution of the Mott-variable range hopping mechanism to the transport phenomenon becomes less significant. A high concentration of electrons gives rise to enhance interaction between the charge carriers mobile.[39] Such behavior can be associated with the effect of the temperature rise on the dynamics of electrons.

Fig. 1(e) presents the variation of $\ln(G_{dc}\cdot T^{1/2})$ as a function of $T^{-1/2}$. In the intermediate temperature interval, the linear slope indicates that the electrical conduction of $Pr_{0.7}Ca_{0.3}Mn_{0.8}Cr_{0.2}O_3$ can be described by the Shklovskii–Efros variable range hopping (SE-VRH) mechanism. In this regime, Coulomb interactions between charge carriers play a major role. So, the temperature dependence of G_{dc} can be explained using SE-VRH model:[65,66]

$$G_{dc}\cdot T = A\exp\left(\frac{-T_0'}{T}\right)^{1/2} \quad (11)$$

A is a pre-exponential factor, whereas the SE-VRH characteristic temperature T_0' is estimated as 3.8×10^4 K. Furthermore, within the same temperature range, the charge transport can be analyzed using the Shimakawa method.[40,67] According to this approach, the electrical conductance can be explained by tunneling mechanisms. For $\theta_D/4 \le T \le \theta_D/2$, the variation of G_{dc} *versus* temperature can be investigated using the relation: $G_{dc}(T) = G_0\cdot(T)^n$ (Fig. 1(f)). The deduced value of the exponent parameter is $n = 7.06$. This suggests that multi-phonon-assisted tunneling processes predominantly govern the conductance.

3.2 Negative temperature coefficient characteristic

A negative temperature coefficient (NTC) thermistor, also known as a negative thermal resistor, is a semiconductor device in which the electrical resistance decreases with increasing temperature. This behavior originates from the effect of temperature on the mobility of the charge carriers. Fig. 2(a) shows the variation of $\ln(R)$ as a function $1/k_BT$ of the $Pr_{0.7}Ca_{0.3}Mn_{0.8}Cr_{0.2}O_3$ oxide. Over the explored temperature region, a linear variation is observed. This behavior is characteristic of materials presenting a pronounced negative temperature coefficient (NTC), in which the electrical resistance decreases with increasing temperature. This indicates the semiconductor nature of the prepared compound. Accordingly, the temperature dependence of the electrical resistance is described by ref. 68 and 69:

$$R = R_0\exp\left(\frac{E_a}{k_BT}\right) \quad (12)$$

R_0 is the resistance at infinite temperature. From the linear Fit of Fig. 2(a), the value of the thermistor constant β is deduced through the relation:[70,71] $\beta = E_a/k_B$, giving a value of $\beta = 1496$ K. Comparing with other systems displaying a thermistor constant (β) varying from 654.68 to 8417.895,[72,73] our elaborated system is a suitable candidate for thermistor applications. In addition, to explore the stability performance of $Pr_{0.7}Ca_{0.3}Mn_{0.8}Cr_{0.2}O_3$

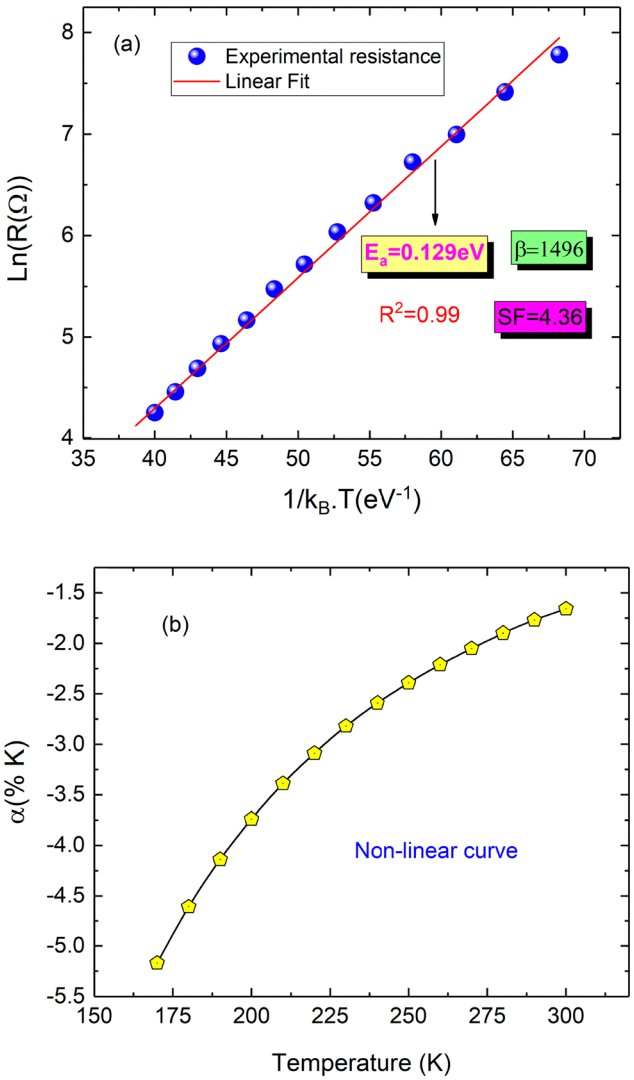

Fig. 2 (a) Evolution of $\ln(R)$ against $1/k_BT$ and the deduced electrical parameters for $Pr_{0.7}Ca_{0.3}Mn_{0.8}Cr_{0.2}O_3$. Temperature dependence of the sensitivity parameter (α) (b).

manganite, the stability factor (SF) value was calculated according to the following relation:[73,74]

$$SF = \log\left(\frac{R_{max}}{R_{min}}\right) \quad (13)$$

For the investigated $Pr_{0.7}Ca_{0.3}Mn_{0.8}Cr_{0.2}O_3$, SF is found to be 4.36. Such a significant value indicates a strong temperature dependence of the electrical resistance response, implying that this compound is a promising candidate for sensor applications.[75,76] Generally, using the factor β, the temperature coefficient or sensitivity parameter (α) can be determined using the following expression:[77]

$$\alpha(T) = -\frac{\beta}{T^2}\times 100 \quad (14)$$

Fig. 2(b) displays the temperature dependence of α for the studied system. The obtained experimental results reveal that α increases in a nonlinear manner, which is a typical behavior

observed in NTC thermistor materials. This nonlinearity is frequently associated with the fast thermal response of sensing materials.[77] In comparison with previously reported results in the literature,[75] the present sample can be considered suitable for thermistor applications. The obtained α value is consistent with those reported by Priyambada Mallick *et al.*, who noted that thermistors exhibiting satisfactory performance generally possess a sensitivity parameter α within the range of −1% to −9%.[75] In the present work, the α values are found to vary between −1% and −4%, demonstrating a good agreement with the desired range. According to previous studies, the variation in the temperature coefficient is mainly attributed to the presence of extrinsic charge carriers in the grain regions, which significantly affect the electrical transport properties.[73]

3.3 The temperature coefficient of resistance

To describe the sensitivity of a compound's electrical resistance to temperature variations, the temperature coefficient of resistance (TCR) is an important parameter. In semiconducting and NTC thermistor materials, the TCR commonly displays negative values, indicating a decrease in the resistance values with increasing temperature.[78–80] Consequently, the TCR analysis is crucial for estimating the potential of materials for temperature-sensing and thermistor applications. The temperature coefficient of resistance (TCR) values are evaluated according to the following expression:[4,78–80]

$$\mathrm{TCR} = \frac{1}{R}\left(\frac{\mathrm{d}R}{\mathrm{d}T}\right) \times 100\% \qquad (15)$$

The temperature coefficient of resistance (TCR %) *versus* temperature for $Pr_{0.7}Ca_{0.3}Mn_{0.8}Cr_{0.2}O_3$ is depicted in Fig. 3. It is evident that the compound exhibits a remarkably high TCR, reaching −20.72 ± 0.5% K^{-1} at T = 100 K, with an activation energy E_a = 0.129 ± 0.003 eV, and a sensitivity parameter β = 1496 ± 35 K. These values indicate a pronounced carrier localization, characteristic of small polaron hopping conduction. Relative to other reported manganites in the literature (see Table 2), the present compound shows a significantly enhanced TCR. For instance for $Sm_{0.45}Pr_{0.1}Sr_{0.45}MnO_3$ (TCR = −7% K^{-1}),[81] $La_{0.7}(Sr_{5/6}Na_{1/6})_{0.3}Mn_{0.7}Ti_{0.3}O_3$ (TCR = −13.36% K^{-1}),[82] $La_{0.14}Nd_{0.35}Sr_{0.3}MnO_3$ (TCR = 2.7% K^{-1}),[83] and $La_{0.7}K_{0.25}Sr_{0.05}MnO_3$ (TCR = 11.9% K^{-1}),[84] $Pr_{0.8}K_{0.1}Na_{0.1}MnO_3$(TCR = −3.79% K^{-1}),[85] $Pr_{0.8}K_{0.15}Na_{0.05}MnO_3$ (TCR = −4.037% K^{-1}),[85] and $Pr_{0.7}Ca_{0.3}Mn_{0.85}Cr_{0.15}O_3$ (~18% K^{-1}).[5] Alongside the previously mentioned oxides, varieties of additional oxide systems exhibiting different crystal structures and transport behaviors have been examined for use in thermistor applications.[86–89] $Ba_3Bi_2Fe_2O_9$ ($\beta \approx 1683$ K)[86] and $KBiFeMnO_5$ ($\beta \approx 4634$ K)[89] are representative examples of defect perovskites and complex oxides that demonstrate comparatively high thermistor constants. Nevertheless, in spite of these elevated β values, their temperature coefficients are either moderate or not expressly indicated, thereby hindering their effectiveness for high-sensitivity temperature sensing applications. The detailed comparison in Table 2, which includes the synthesis method, peak TCR temperature, activation energy (E_a), and sensitivity parameter (β), demonstrates that the present sample achieves an optimal combination of high TCR and moderate activation energy. This combination enables a rapid response and dependable performance across the operating temperature range, highlighting the material's suitability for low-temperature sensing. Compared with the TCR values reported for the above-mentioned oxides, the $Pr_{0.7}Ca_{0.3}Mn_{0.8}Cr_{0.2}O_3$ sample demonstrates significant potential for applications in low-temperature sensors, such as detectors.

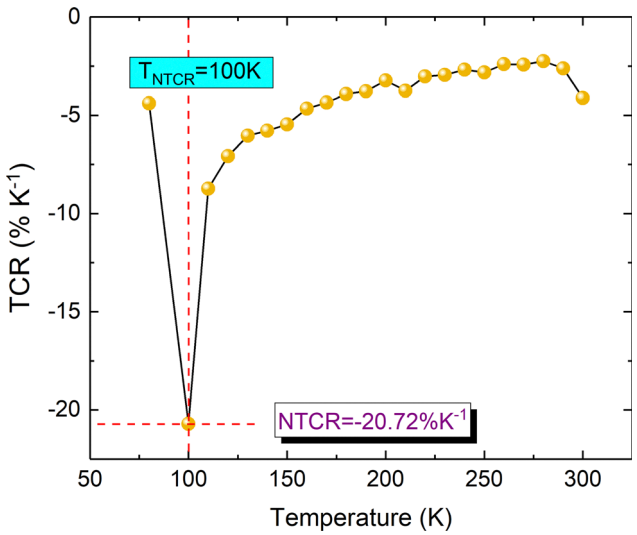

Fig. 3 Variation of the temperature coefficient of resistance (TCR) against temperature $Pr_{0.7}Ca_{0.3}Mn_{0.8}Cr_{0.2}O_3$ compound.

3.4 AC-conductance study

3.4.1 Effect of the frequency variation on the electrical behavior. The temperature dependence of the electrical conductance for $Pr_{0.7}Ca_{0.3}Mn_{0.8}Cr_{0.2}O_3$ at different frequencies is shown in Fig. 4(a). For all the chosen frequency values, it is clearly observed that the conductance values increase with increasing temperature. Such behavior confirms the semiconductor character of the investigated compound. This behavior arises from the existence of cation–anion–cation interactions within the entire temperature domain examined. As a function of increasing temperature, each conductance curve can be split into two distinct domains. Below T_d = 170 K, a noticeable impact on the frequency increase on the electrical conductance is observed at very low temperatures. Indeed, the conductance response is found to increase proportionally with frequency. In such temperature regions, the transport properties of $Pr_{0.7}Ca_{0.3}Mn_{0.8}Cr_{0.2}O_3$ are dominated by the Mott-VRH conduction process. Therefore, increasing the frequency has a negligible influence on the cationic disorder of the mentioned system. For $T > T_d$ = 170 K, the electrical conductance is solely controlled by temperature variation. In fact, the rise in frequency does not influence its behavior or order.

Fig. 4(b) presents the variation of $\ln(G_{ac}\cdot T)$ *versus* $1/k_BT$. This kind of representation allows us to deduce the activation energy (E_a) value in different temperature intervals and at multiple

Table 2 Comparison of thermistor parameters of the studied material with comparable oxide-based thermistors from literature

Materials	Synthesis method	TCR (% K^{-1})	Peak TCR temperature (K)	E_a (eV)	β (K)	Ref.
$Pr_{0.7}Ca_{0.3}Mn_{0.8}Cr_{0.2}O_3$	Solid-state reaction	−20.72	100	0.129	1496	This work
$Sm_{0.45}Pr_{0.1}Sr_{0.45}MnO_3$	Solid-state reaction	−7	160	0.168	—	81
$La_{0.7}(Sr_{5/6}Na_{1/6})_{0.3}Mn_{0.7}Ti_{0.3}O_3$	Solid-state reaction	−13.36	115	0.196	—	82
$La_{0.14}Nd_{0.35}Sr_{0.3}MnO_3$	Solid-state reaction	2.7	289	—	—	83
$La_{0.7}K_{0.25}Sr_{0.05}MnO_3$	Sol–gel spin-coating technique	11.9	291.2	—	—	84
$Pr_{0.8}K_{0.1}Na_{0.1}MnO_3$	Sol–gel method	−3.79	200	—	—	85
$Pr_{0.8}K_{0.15}Na_{0.05}MnO_3$	Sol–gel method	−4.037	180	—	—	85
$Pr_{0.7}Ca_{0.3}Mn_{0.85}Cr_{0.15}O_3$	Solid-state reaction	18	90	0.115	1350	5
$Ba_3Bi_2Fe_2O_9$	Solid-state sintering technique	—	—	—	≈1683	86
$KBiFeMnO_5$	Solid-state sintering technique	—	—	≈0.399	≈4634	89

frequencies. It also highlights the effect of frequency on E_a. Thus, the activation energy value for each selected frequency was determined from the observed slopes. At low frequencies, the calculated activation energy is found to be E_a = 170 meV, which is very close to the value obtained from the DC-conductance analysis (E_a = 178 meV) within the same temperature range (Fig. 1(b)). This close indicates a strong correlation between AC and DC conductance, suggesting that they originate from the same mechanism. Fig. 4(c) displays the frequency dependence of the disorder E_D and hopping E_H energies. From the variation of E_D, it is observed that the increase in frequency leads to decreased E_D values, which is in agreement with Miller–Abrahams theory:[47,90]

$$E_D = \frac{0.3e^2}{\varepsilon_s \times R_{hop}} \quad (16)$$

The factors e and ε_s present respectively the electronic charge and the static dielectric constant. The variation in the disorder energy with frequency may be associated with a modification in the average distance between the hop centers (R_{hop}). However, an increase in the hopping energy (E_H) with rising frequency is observed. Following the theories of Mott *et al.*,[39,40,42,43] E_H can be determined using the following equation:

$$E_H = \frac{E_p}{2} = \frac{e^2}{4\varepsilon_p}\left(\frac{1}{R_{pol}} - \frac{1}{R_{hop}}\right) \quad (17)$$

R_{pol} is the radius of polaron and ε_p is the effective dielectric constant.

3.4.2 Conductance spectrum analysis. To elucidate the charge transport mechanism and explain the origin of the electrical conduction in the AC region, the investigation of the electrical conductance as a function of frequency is an effective approach. Such measurements provide valuable insight into the models governing transport properties. For manganite materials, it has been widely reported that the conductance spectra in the dispersive zone generally follow Jonscher's or double Jonscher power laws. Within this framework, the dominant conduction mechanisms associated with charge carrier displacement between sites can be identified through the analysis of the frequency exponent s. In the present section, the frequency dependence of the ac-conductance (G_{ac}) for the investigated $Pr_{0.7}Ca_{0.3}Mn_{0.8}Cr_{0.2}O_3$ is shown in Fig. 5(a). As a function of the frequency rise, each conductance curve is characterized by the presence of two distinct regions. At low frequencies, the ac-conductance remains almost constant, indicating that the transport process is not influenced by frequency variation. Hence, the conductance spectrum shows a DC plateau, which arises from long-range charge transport.[8,91,92] This behavior is generally associated to the thermally activated nature of the small polaron hopping. At high frequencies, and in the temperature range [80–280 K], each conductance spectrum exhibits a single dispersive region. In this region, G_{ac} depends strongly on frequency and increases as the frequency rises. Thus, the Jonscher power law (JPL) is valid for explaining the electrical response of the system, expressed as:[57,93]

$$G_{ac} = G_{dc} + A\omega^s \quad (18)$$

The parameter s is the frequency exponent, which varies with temperature. It expresses the coupling between the charge carriers and the lattice. For recent oxide and brownmillerite-based materials, authors have reported similar conductivity spectra, suitable for thermistor and electronic applications.[94–96] For example, in their study of the defect brownmillerite $LiBiFeMnO_5$, Panda *et al.*[94] reported conductivity spectra characterized by a low-frequency plateau, ascribed to long-range charge transport, accompanied by a dispersive high-frequency region associated with thermally activated hopping among localized states. A JPL-type response was also observed over a wide temperature range in complex molybdate materials such as Sr–Bi–Mo–O ceramics,[96] where the dispersive range was attributed to short-range hopping of charge carriers across grain boundaries and defect sites. These results suggest that the JPL is an effective approach for describing the AC conductivity of different material classes, such as manganites. Beyond T = 280 K, a decrease in the conductance is observed. Although this behavior may appears metallic-like behavior, however, in polaronic manganites, it should be interpreted with precaution. In fact, the reduction in the electrical conductance with increasing temperature can be related to strengthened carrier scattering. This behavior occurs due to strong electron–phonon interactions, which reduce carrier mobility. As the temperature increases, the scattering mechanism becomes more pronounced. This leads to a hindrance of charge transport and therefore to the observed decrease in the conductance. In this temperature range, the transport mechanism wanders a crossover from a thermally activated regime, commonly described by small polaron hopping,[39,40] toward a regime of delocalized carriers with significant scattering, as widely reported in manganite systems.[4,6]

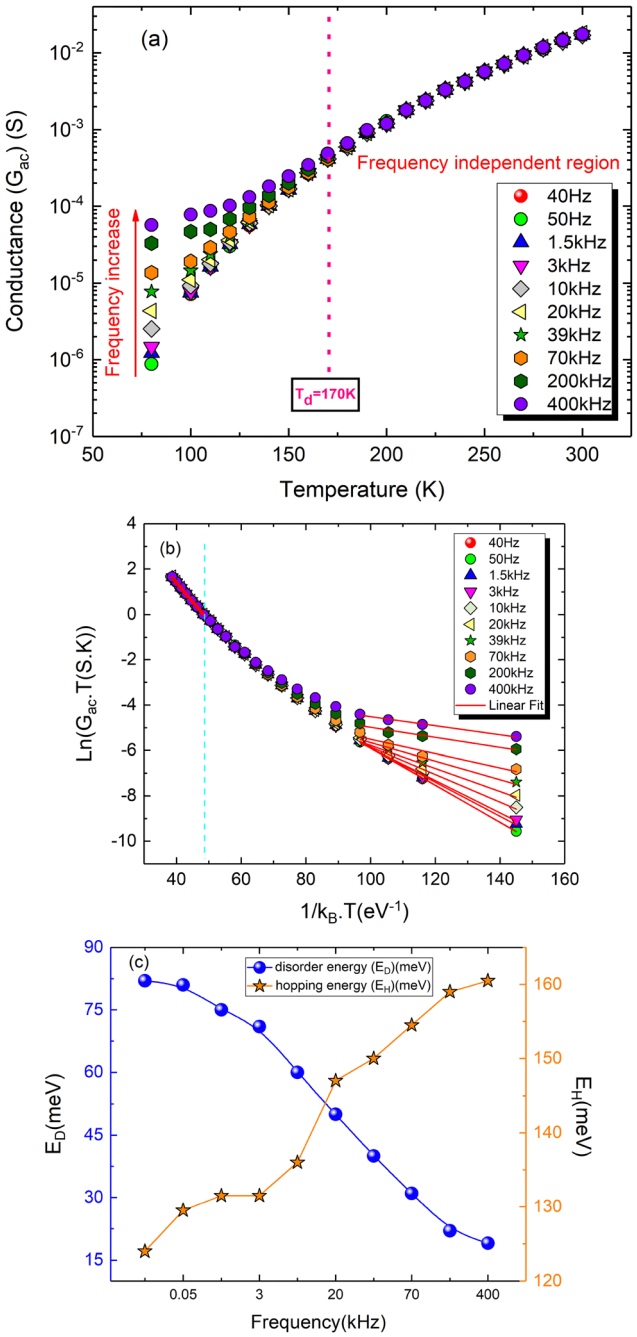

Fig. 4 (a) Temperature dependence of G_{ac} at selected frequencies for $Pr_{0.7}Ca_{0.3}Mn_{0.8}Cr_{0.2}O_3$. Plot of ln($G_{ac}$·$T$) against 1/$k_BT$ (b). Frequency dependence of the disorder E_D and hopping E_H energies (c).

Such transition is also supported by the change in the temperature dependence of conductance, such as variation in the slope, which indicates a shift from localized to partially delocalized charge transport. Based on the above results, the ac-conductance is well fitted by the Drude model:[97]

$$G_{ac} = \frac{G_{dc}}{1 + \omega^2 \tau_s^2} \quad (19)$$

The parameter τ_s is the time between two consecutive collisions.

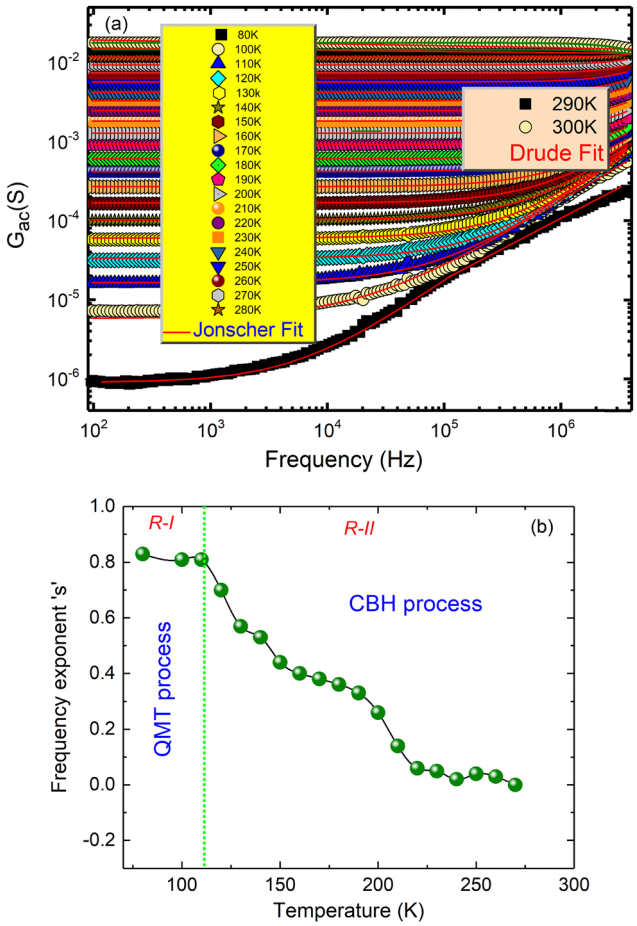

Fig. 5 (a) Frequency dependence of AC-conductance (G_{ac}) for $Pr_{0.7}Ca_{0.3}Mn_{0.8}Cr_{0.2}O_3$. Temperature dependence of the frequency exponent 's' (b).

In accordance with the Drude model, the metallic-like behavior observed in $Pr_{0.7}Ca_{0.3}Mn_{0.8}Cr_{0.2}O_3$ manganite, at elevated frequencies can be associated with the polaronic charge carriers. This behavior is further influenced by the double-exchange mechanism, which promotes the creation of effectively free hopping electrons. Such a process improves free electron collisions and strengthens the direct interaction between the Mn cations. To clarify the origin of the conductance increase in the dispersive zone and to identify the dominant AC conduction processes, the temperature dependence of the frequency exponent 's' is shown in Fig. 5(b). According to the found results in ref. 6, 8 and 61, it is identified that the transport properties can be dominated by the contribution of both tunneling and hopping conduction models. As shown in Fig. 5(b), that the obtained values of 's' are less than the unity indicating that the charge carriers transport occurs through translation motion accompanied by sudden hopping. In the investigated temperature region, it is clearly observed that the conductance increase in the dispersive range is mainly due to the contribution of two dissimilar conduction mechanisms. In the first region (R-I), corresponding to the temperature range T = 80–110 K, the frequency exponent's' appears temperature independent. It

achieved a value of $s = 0.81$. This is in good agreement with the quantum–mechanical tunneling process (QMT). As reported in ref. 27, 47 and 61 that the temperature independent of the tunneling distance and the constancy of the frequency exponent '*s*' with temperature may be the responsible for the occurrence of the QMT model. In the second region (R-II), defined over the temperature range $T = 110$–280 K, the parameter '*s*' is found to increase with decreasing temperature, reaching a value of 0.8 at $T = 110$ K. In such case, we can assume that the correlated barrier hopping (CBH) model can be considered as the appropriate model for describing the charge transport properties of the investigated system within this temperature region. The same evolution has also been reported in Co-PCMO manganites.[8]

4. Conclusion

A comprehensive investigation of the transport properties of $Pr_{0.7}Ca_{0.3}Mn_{0.8}Cr_{0.2}O_3$ has been carried out to evaluate its potential in thermistor and sensor applications. The obtained results demonstrate that $Pr_{0.7}Ca_{0.3}Mn_{0.8}Cr_{0.2}O_3$ exhibits not only well-defined semiconducting transport governed by non-adiabatic small polaron hopping and variable range hopping mechanisms, but also promising thermistor characteristics. The relatively high TCR value obtained at low temperature, together with favorable sensitivity (β, α) and stability (SF) parameters, underscores the potential of this compound for thermal sensing applications. The observed dispersive conductance range arises from the combined contribution of both hopping and tunneling processes, including QMT, and the CBH models. Importantly, the present study goes beyond conventional transport modeling by establishing a clear correlation between the underlying conduction processes and the resulting functional performance. This approach provides new insight into the design and optimization of manganite-based materials for thermistor devices, thereby offering a benefit compared to previous investigations on similar systems.

Conflicts of interest

The authors declare no conflicts of interest.

Data availability

All the data that support this research are included within the article.

References

1 O. Vitayaya, B. Kurniawan and M. Manawan, Factors Affecting the Resistivity and Colossal Magnetoresistance (CMR) of Manganite Materials, *J. Mater. Chem. C*, 2026, **14**, 2134–2173.
2 S. S. S. A. Aziz, N. A. Amaran, R. Rajmi, S. S. Olalekan, Z. Mohamed and N. Ibrahim, Influence of Cr substitution on electrical and dielectric properties of monovalent doped Pr-based manganites, AIMS, *Mater. Sci.*, 2025, **12**, 909.
3 F. Q. Batista, D. J. Lopes, O. J. Dura, S. M. Mikhalev, G. Constantinescudd, F. M. Costa, A. V. Kovalevsky and N. M. Ferreira, Laser processing of calcium manganite-based materials for thermoelectric generators, *Ceram. Int.*, 2025, **51**(30), 62231.
4 R. Hanen, Y. Moualhi, A. Selmi and H. Rahmouni, Mott and Jonscher Models for conductance analysis of Chromium-PCMO oxide: thermistor parameters test for thermo-sensitive applications, *Ceram. Int.*, 2026, **52**(11), 15681–15691.
5 Y. Moualhi, A. Selmi and H. Rahmouni, Inductive-like Nyquist responses and tunable transport mechanisms in Cr-Doped manganites: toward next-generation sensors and electronic devices, *Ceram. Int.*, 2025, **52**, 6610.
6 Y. Moualhi, M. Alruwaili, M. A. Alamri, M. Alhabradi, S. Elkossi, H. Belmabrouk and H. Rahmouni, Motivating electrical characteristics of $La_{0.7}(Sr_{5/6}Na_{1/6})_{0.3}MnO_3$ and possibility of its application as direct temperature switcher in electronic devices, *Mater. Chem. Phys.*, 2025, **345**, 131205.
7 A. Ghodhbani, Y. Moualhi, A. Midouni, M. A. Albedah, H. Rahmouni, K. Khirouni and H. Belmabrouk, Tunable electrical transport and conduction pathways in $La_{0.8}Ca_{0.2}Mn_{0.5}Cu_{0.5}O_3$: toward bolometric applications, *Mater. Sci. Eng., B*, 2026, **327**, 119295.
8 R. Hanen, Y. Moualhi, H. Rahmouni and K. Khirouni, Effect of substituting manganese by few cobalt content in the transport properties of Pr/Ca based manganite, *R. Soc. Chem. Adv.*, 2024, **35**, 1373.
9 A. Miri, M. H. Ehsani and S. Esmaeili, Structural and electrical properties of gadolinium-substituted $La_{0.6-x}Gd_xSr_{0.4}MnO_3$ (x = 0–0.3), *Eur. Phys. J. Plus*, 2023, **138**, 1.
10 H. E. Sekrafi, A. B. J. Kharrat, M. A. Wederni, N. Chniba-Boudjada, K. Khirouni and W. Boujelben, Impact of low titanium concentration on the structural electrical and dielectric properties of $Pr_{0.75}Bi_{0.05}Sr_{0.1}Ba_{0.1}Mn_{1-x}Ti_xO_3$ (x = 0, 0.04) compounds, *J. Mater. Sci.: Mater. Electron.*, 2019, **30**, 89.
11 X. Deng, J. Guo, S. Ding, Y. Xie, H. Zhang, H. Liu, Q. Chen and Y. Li, Influence of Nd doping on the electrical and magnetoresistance properties of $La_{0.7}Ca_{0.3}MnO_3$ ceramics, *Ceram. Int.*, 2025, **51**(9), 11560.
12 Z. Dong, M. Shao, Y. Li, L. Li, W. Yang, J. Xie and J. Yang, Enhanced anisotropic magnetoresistance in $La_{0.7-x}Sm_xCa_{0.3}MnO_3$ through lattice distortion control for magnetic sensors, *Ceram. Int.*, 2025, **51**(8), 10887.
13 Z. C. Xia, S. L. Yuan, W. Feng, L. J. Zhang, G. H. Zang, J. Tang, L. Liu, D. W. Liu, Q. H. Zheng, L. Chen, Z. H. Fang, S. Liu and C. Q. Tang, Magnetoresistance and transport properties of different impurity doped $La_{0.67}Ca_{0.33}MnO_3$ composite, *Solid State Commun.*, 2003, **127**, 567.
14 Q. Zhang, L. Yin, W. Mi and X. Wang, Large Spatial Spin Polarization at Benzene/$La_{2/3}Sr_{1/3}MnO_3$Spinterface:Toward Organic Spintronic Devices, *J. Phys. Chem. C*, 2016, **120**, 6156.

15 D. Robinson, C. Sepulveda, E. J. Delgado, O. Peña, J. L. G. Fierro and G. Pecchi, Electronic properties and catalytic performance for DME combustion of lanthanum manganites with partial B-site substitution, *J. Catal.*, 2016, **338**, 47.

16 H. Zhou, H. Wang, Y. Chen, K. Li and X. Yao, Low temperature sintering and microwave dielectric properties of $Ba_3Ti_5Nb_6O_{28}$ ceramics with $BaCu(B_2O_5)$ additions, *Mater. Chem. Phys.*, 2009, **113**, 1.

17 Y. Moualhi, M. Smari and H. Rahmouni, Understanding the charge carriers dynamics in the $La_{0.55}Ca_{0.45}Mn_{0.8}Nb_{0.2}O_3$ perovskite: scaling of electrical conductivity spectra, *RSC Adv.*, 2023, **13**, 30010.

18 Y. Moualhi, R. M'nassri, M. M. Nofal, H. Rahmouni, A. Selmi, M. Gassoumi, N. Chniba-Boudjada, K. Khirouni and A. Cheikrouhou, Influence of Fe doping on physical properties of charge ordered praseodymium-calcium-manganite material, *Eur. Phys. J. Plus*, 2020, **135**, 809.

19 A. K. Saw, G. Channagoudra and S. Hunagund, *et al.*, Study of transport, magnetic and magnetocaloric properties in Sr^{2+} substituted praseodymium manganite, *Mater. Res. Express*, 2019, **7**, 016105.

20 R. Shaiboub and A. Hamed, Effect of Mn-Site Doping on the Magnetic Properties of the $La_{2/3}Sr_{1/3}Mn_{1-x}In_xO_3$ Manganite Perovskite, *J. Pure Appl. Sci.*, 2026, 105–109.

21 Y. K. Lakshmi, G. Venkataiaha, M. Vithal and P. V. Reddy, Magnetic and electrical behavior of $La_{1-x}A_xMnO_3$ (A = Li, Na, K and Rb) manganites, *Phys. B*, 2008, **403**, 3059.

22 V. K. Haripriya, A. George and K. A. Malini, Effect of Synthesis Route on the Structural and Electrical Properties of Co Substituted Ni–Mn Oxide Based NTC Thermistors, *Curr. Appl. Phys.*, 2026, **84**, 88–96.

23 L. Vedmid', O. Fedorova, S. Belyakov and V. Balakireva, Effect of substitution in A and B sublattices on the structural, magnetic, electrical properties and microstructure of $EuMnO_3$, *Emergent Mater.*, 2025, **8**(6), 4843–4861.

24 K. Navin and R. Kurchania, A comparative study of the structural, magnetic transport and electrochemical properties of $La_{0.7}Sr_{0.3}MnO_3$ synthesized by different chemical routes, *Appl. Phys. A: Mater. Sci. Process.*, 2020, **126**, 100.

25 D. Grossin and J. G. Noudem, Synthesis of fine $La_{0.8}Sr_{0.2}MnO_3$ powder by different ways, *Solid State Sci.*, 2004, **6**, 939.

26 P. R. Koushalya and K. N. Anuradha, Effect of 'a' and 'b' site substitution on magnetic properties of bulk and nanoparticles of $Pr_{0.57}Ca_{0.43}MnO_3$ manganite, *AIP Conf. Proc.*, 2020, **2274**, 020001.

27 Y. Moualhi, R. M'nassri, H. Rahmouni, M. Gassoumi and K. Khirouni, Possibility of controlling the conduction mechanism by choosing a specific doping element in a praseodymium manganite system, *RSC Adv.*, 2020, **10**, 33868.

28 N. J. Nor-Azah, K. Muhammad-Aizat and R. Abd-Shukor, Constructive effects of Fe-doping on the temperature coefficient of resistance and magnetoresistance of $La_{0.7}Ca_{0.3}Mn_{1-x}Fe_xO_3$, *Ceram. Int.*, 2025, **52**(4), 4268–4280.

29 D. Toyganözü, S. Kılıç Çetin, G. Akça and A. Ekicibil, Enhanced magnetocaloric performance with room-temperature transition in Bi-substituted $La_{0.65}Ca_{0.20}Pb_{0.15}Mn_{1-x}Bi_xO_3$ (x = 0.0, 0.01, 0.03, and 0.05) perovskites, *J. Mater. Sci.: Mater. Electron.*, 2026, **37**(2), 129.

30 A. Selmi, A. Bettaibi, H. Rahmouni, R. M'nassri, N. Chniba Boudjada, A. Cheikhrouhou and K. Khirouni, Physical properties of 20% Cr-doped $Pr_{0.7}Ca_{0.3}MnO_3$ perovskite, *Ceram. Int.*, 2015, **41**, 11221.

31 S. Lv, Y. Jiang, M. Liu, J. Li, Z. Zhao, X. Wang, B. Li, S. Liu, F. Cui, D. Lv, Y. Yang and L. Xia, Vacancy-mediated electromagnetic loss tuning in Cr-doped lanthanum manganite perovskites for broadband and high-intensity microwave absorption, *J. Adv. Ceram.*, 2025, **14**(12), 9221202.

32 N. Kumar, S. Pant and K. Singh, Effect of Cr, Fe, and Co doping on the structural, transport, and magnetic properties of $La_{0.7}Ca_{0.3}Mn_{1-x}M_xO_3$ (M = Cr, Fe, Co) compounds, *J. Magn. Magn. Mater.*, 2025, 173759.

33 W. L. Teo, S. Shamsuddin, S. K. Muzakir and M. B. Rodhuan, Room Temperature Structural and Electrical Studies on Jahn–Teller Distortions Signal Induced by Cr and Co Doping in $Pr_{0.75}Na_{0.2}Ag_{0.05}Mn_{1-x}M_xO_3$ Perovskite Manganites, *Eng., Technol. Appl. Sci. Res.*, 2025, **15**(5), 27244–27249.

34 S. Sumaiyah, N. Ibrahim, Z. Mohamed, R. Rozilah, J. Kazmi, A. Masood and M. Ali, Electrical, magnetic, and magnetoresistance studies in chromium-doped Pr-based manganites, *J. Mater. Sci.: Mater. Electron.*, 2024, **35**, 1336.

35 S. Pal, S. Biswas, R. Nag and E. Bose, Hopping Transport and Spin-Polarized Tunneling Mechanism in Cr-Doped $Gd_{0.7}Ca_{0.3}Mn_{1-x}Cr_xO_3$ (x = 0.0–0.5), *J. Supercond.*, 2017, **30**, 2505.

36 S. O. Manjunatha, A. Rao, P. D. Babu, T. Chand and G. S. Okram, Electric, magnetic,and thermo-electric properties of Cr doped $La_{0.8}Ca_{0.2}Mn_{1-x}Cr_xMnO_3$ manganites, *Solid State Commun.*, 2016, **239**, 37.

37 K. Abdouli, F. Hassini, W. Cherif, P. R. Prezas, M. P. F. Graça, M. A. Valent, O. Messaoudi, S. Elgharbi, A. Dhahri and L. Manai, Investigation of the structural, electrical, anddielectric properties of $La_{0.5}Sm_{0.2}Sr_{0.3}Mn_{1-x}Cr_xO_3$ for electrical application, *RSC Adv.*, 2022, **12**, 16805.

38 S. Cao, W. Li, J. Zhang, B. Kang, T. Gao and C. Jing, Cr-doping-induced phase separation and MR effect in the manganite $Pr_{0.5}Ca_{0.5}Mn_{1-x}Cr_xO_3$ system, *J. Appl. Phys.*, 2007, **102**, 053909.

39 N. F. Mott, The origin of some ideas on non-crystalline materials, *J. Non-Cryst. Solids*, 1978, **28**, 147.

40 N. F. Mott, Conduction in glasses containing transition metal ions, *J. Non-Cryst. Solids*, 1968, **1**, 1.

41 I. G. Austin and N. F. Mott, Polarons in crystalline and non-crystalline materials, *Adv. Phys.*, 1969, **18**, 41.

42 N. F. Mott, Conduction in non-crystalline materials, *Philos. Mag.*, 1969, **19**, 835.

43 N. F. Mott, Polarons, *Mater. Res. Bull.*, 1978, **13**, 1389.

44 A. Ghosh and M. Sural, Conductivity spectra of sodium fluorozirconate glasses, *J. Chem. Phys.*, 2001, **114**, 3243.

45 A. Ghosh and A. Pan, Scaling of the conductivity spectra in ionic glasses: dependence on the structure, *Phys. Rev. Lett.*, 2000, **84**, 2188.
46 S. R. Elliott, A. C. conduction in amorphous chalcogenide and pnictide semiconductors, *Adv. Phys.*, 1987, **36**, 135.
47 Y. Moualhi, H. Rahmouni and K. Khirouni, Usefulness of theoretical approaches and experiential conductivity measurements for understanding manganite-transport mechanisms, *Results Phys.*, 2020, **19**, 103570.
48 S. R. Elliott and F. E. G. Henn, Application of the Anderson–Stuart model to the AC conduction of ionically conducting materials, *J. Non-Cryst. Solids*, 1990, **116**, 179.
49 T. Tang, Q. Q. Cao, K. M. Gu, H. Y. Xu, S. Y. Zhang and Y. W. Du, Giant magnetoresistance of the $La_{1-x}Ag_xMnO_3$ polycrystalline inhomogeneous granular system, *Appl. Phys. Lett.*, 2000, **77**, 723.
50 L. Pi, M. Hervieu, A. Maignan, C. Martin and B. Raveau, Structural and magnetic phase diagram and room temperature CMR effect of$La_{1-x}Ag_xMnO_3$, *Solid State Commun.*, 2003, **126**, 229.
51 C. Zener, Interaction between the d-shells in the transition metals. II. Ferromagnetic compounds of manganese with perovskite structure, *Phys. Rev.*, 1951, **82**, 403.
52 S. Sumaiyah, N. Ibrahim, Z. Mohamed, R. Rozilah, J. Kazmi, A. Masood and M. Ali, Electrical, magnetic, and magnetoresistance studies in chromium-doped Pr-based manganites, *J. Mater. Sci.: Mater. Electron.*, 2024, **35**, 1336.
53 S. Bhattacharya, R. K. Mukherjee, B. K. Chaudhuri and H. D. Yang, Effect of Li doping on the magnetotransport properties of $La_{0.7}Ca_{0.3-y}Li_yMnO_3$ system: decrease of metal–insulator transition temperature, *Appl. Phys. Lett.*, 2003, **82**, 4101.
54 T. Holstein, Studies of polaron motion: part II, the ''small'', *Polaron*, 1959, **8**, 343.
55 T. Holstein, Studies of polaron motion: part I. The molecular-crystal model, *Physics*, 1959, **8**, 325.
56 Y. Moualhi, M. Javed, N. Akbar and H. Rahmouni, Carrier motion origins and dual-permittivity behavior in $FeNi_2O_4$: dielectric resonance, epsilon-near-zero, polarization effects, and possible advanced electromagnetic applications, *Mater. Sci. Semicond. Process.*, 2025, **200**, 110000.
57 A. K. Jonscher and M. S. Frost, Weakly frequency-dependent electrical conductivity in a chalcogenide glass, *Thin Solid Films*, 1976, **37**, 267.
58 H. Ahmed, S. Khan, W. Khan, R. Nongjai and I. Khan, Adiabatic to non-adiabatic change in conduction mechanism of Zn doped $La_{0.67}Sr_{0.33}MnO_3$ perovskite, *J. Alloys Compd.*, 2013, **563**, 12.
59 R. N. Jadhav, S. N. Mathad and V. Puri, Studies on the properties of $Ni_{0.6}Cu_{0.4}Mn_2O_4$ NTC ceramic due to Fe doping, *Ceram. Int.*, 2012, **38**, 5181.
60 A. Deppeler and A. J. Millis, Electron-phonon interactions in correlated systems: adiabatic expansion of the dynamical mean-field theory, *Phys. Rev. B: Condens. Matter Mater. Phys.*, 2002, **65**, 100301.
61 A. Ghodhbani, Y. Moualhi, W. Dimassi, R. M'nassri, H. Rahmouni and K. Khirouni, Contribution of strong electron-phonon interaction in the transport properties of $La_{0.8}Ca_{0.2}Mn_{0.5}Ni_{0.5}O_3$ system, *Phys. B*, 2024, **683**, 415964.
62 G. Zhao, V. Smolyaninova, W. Prellier and H. Keller, Electrical transport in the ferromagnetic state of manganites: small-polaron metallic conduction at low temperatures, *Phys. Rev. Lett.*, 2000, **84**, 6086.
63 Y. D. Zhang, T. L. Phan, D. S. Yang and S. C. Yu, Local structure and magnetocaloric effect for $La_{0.7}Sr_{0.3}Mn_{1-x}Ni_xO_3$, *Curr. Appl. Phys.*, 2012, **12**, 803.
64 P. Nagels, *Electronic transport in amorphous semiconductors, Amorphous Semiconductors*, Springer, Berlin, Heidelberg, 1979, p. 113.
65 B. I. Shklovskii and A. L. Efros, *Electronic Properties of Doped Semiconductors*, Springer, Berlin, 1984.
66 A. L. Efros and B. I. Shklovskii, Coulomb interaction in disordered systems with localized electronic states, *Mod. Problems Condens. Matter Sci.*, 1985, **10**, 409.
67 Y. Moualhi, M. M. Nofal, R. M'nassri, H. Rahmouni, A. Selmi, M. Gassoumi, K. Khirouni and A. Cheikrouhou, Double Jonscher response and contribution of multiple mechanisms in electrical conductivity processes of Fe–PrCaMnO ceramic, *Ceram. Int.*, 2020, **46**, 1601.
68 S. R. Elliott and F. E. G. Henn, Application of the Anderson-Stuart model to the AC conduction of ionically conducting materials, *J. Non-Cryst. Solids*, 1990, **116**, 179.
69 G. N. Greaves, Small polaron conduction in V_2O_5 P_2O_5 glasses, *J. Non-Cryst. Solids*, 1973, **11**, 427.
70 C. Yuan, X. Liu, M. Liang, C. Zhou and H. Wang, Electrical properties of Sr–Bi–Mn–Fe–O thick-film NTC thermistors prepared by screen printing, *Sens. Actuators, A*, 2011, **167**, 291.
71 Z. P. Nenova and T. G. Nenov, Linearization Circuit of the Thermistor Connection, *IEEE Trans. Instrum. Meas.*, 2009, **58**, 441.
72 P. Mallick, S. Kumari Yadav, S. K. Satpathy, B. Behera, S. Moharana and S. Sagadevan, Impact of gadolinium doping on $BiFeO_3$–$PbZrO_3$ for energy storage applications: structural, microstructural, and thermistor properties, *Inorg. Chem. Commun.*, 2024, **166**, 112626.
73 A. K. Sahu, P. Mallick, S. K. Satpathy and B. Behera, Effect on structural, electrical and temperature sensing behavior of neodymium doped bismuth ferrite, *Adv. Mater. Lett.*, 2021, **12**(7), 1.
74 S. Jagtap, S. Rane, U. Mulik and D. Amalnerkar, Thick film NTC thermistor for wide range of temperature sensing, *Microelectron. Int.*, 2007, **24**, 7.
75 Y. Moualhi, H. Rahmouni and F. Bahri, Doublet doped titanate ferroelectric system for capacitors and NTC thermistor applications, *Sens. Actuators, A*, 2024, **377**, 115596.
76 Y. Q. Gao, Z. M. Huang, Y. Hou, J. Wu, W. Zhou, C. Ou Yang, J. G. Huang, J. C. Tong and J. H. Chu, Structural and electrical properties of $Mn_{1.56}Co_{0.96}Ni_{0.48}O_4$ NTC thermistor films, *Mater. Sci. Eng., B*, 2014, **185**, 74.
77 B. Zhang, Q. Zhao, A. Chang, H. Ye, S. Chen and Y. Wu, New negative temperature coefficient thermistor ceramics in Mn-doped $CaCu_{3-x}Mn_xTi_4O_{12}$ $(0 \leq x \leq 1)$ system, *Ceram. Int.*, 2014, **40**, 11221.

78 I. Ouni, Y. Moualhi and H. Rahmouni, Thermistor and capacitor parameter analysis through electrical and dielectric investigations of manganite systems for technological applications, *Sens. Actuators, A*, 2025, **384**, 116300.

79 S. Vadnala, T. D. Rao, P. Pal and S. Asthana, Study of structural effect on Eu-substituted LSMO manganite for high temperature coefficient of resistance, *Phys. B*, 2014, **448**, 277.

80 I. Ouni, Y. Moualhi and H. Rahmouni, Regarding application in sensor; a comparative study of electrical properties of $Pr_{0.8}X_{0.2}MnO_3$ (X = Na and X = K) ceramics, *Inorg. Chem. Commun.*, 2025, **179**, 114756.

81 Y. Moualhi and H. Rahmouni, Influence of the structural disorder and applied bias voltage variations on the hopping conduction mechanisms, scattering processes, and temperature coefficient of resistance characteristics of $Sm_{0.55-x}Pr_xSr_{0.45}MnO_3$ $(0 \leq x \leq 0.4)$ ceramics, *Mater. Chem. Phys.*, 2025, **332**, 130185.

82 Y. Moualhi, M. A. Alamri, A. Jbeli, N. Ahmed Althumairi, S. El Kossi, R. Ayed Brahem and H. Rahmouni, Elaboration of La(Sr/Na)Mn(Ti)O_3 ceramic, structural, and morphological investigations, and contribution of direct and indirect interactions on transport properties, *Ceram. Int.*, 2024, **50**, 16587.

83 C. Wang, H. Zhang, Y. Li, S. Yang and Q. Chen, Effect of Y doping on transport properties of $La_{0.8}Sr_{0.2}MnO_3$ polycrystalline ceramics, *Ceram. Int.*, 2020, **46**, 11950.

84 X. Guan, H. Li, Z. Yu, X. Yu, S. Jin, X. Gu and X. Liu, Tuning room-temperature TCR of $La_{0.7}K_{0.3-x}Sr_xMnO_3$ $(0.00 \leq x \leq 0.3)$ films by K and Sr co-occupying A-site, *Appl. Phys. Lett.*, 2022, **121**, 202203.

85 I. Ouni and H. Rahmouni, TCR parameter study for examining the possibility of the usefulness of perovskite $Pr_{0.8}K_{0.2-x}Na_xMnO_3$ (x = 0.0, 0.05 and 0.1) systems for thermistor and bolometer applications, *Mater. Adv.*, 2026, **7**, 1537–1551.

86 D. Panda, S. S. Hota, S. K. Dash, D. K. Patel and R. N. P. Choudhary, Development of a lead-free colossal dielectric material barium bismuth ferrous oxide for electronic devices, *Ceram. Int.*, 2024, **50**, 20098.

87 D. Panda, S. S. Hota and R. N. P. Choudhary, Synthesis of a scheelite barium molybdate: structural, topological, electrical, and transport properties for negative temperature coefficient thermistor application, *J. Solid State Chem.*, 2024, **331**, 124531.

88 D. Panda, S. S. Hota and R. N. P. Choudhary, Investigation of structural, topological, and electrical properties of scheelite strontium molybdate for electronic devices, *Inorg. Chem. Commun.*, 2023, **158**, 111501.

89 D. Panda, S. S. Hota and R. N. P. Choudhary, Investigation of the structural, surface topographical, fractal, capacitive, and electrical properties of a defect brownmillerite perovskite material $KBiFeMnO_5$ for electronic devices, *RSC Adv.*, 2024, **14**(5), 3400.

90 A. Miller and E. Abrahams, Impurity conduction at low concentrations, *Phys. Rev.*, 1960, **120**, 745.

91 K. M. Sangwan, N. Ahlawat, S. Rani, S. Rani and R. S. Kundu, Influence of Mn doping on electrical conductivity of lead free $BaZrTiO_3$ perovskite ceramic, *Ceram. Int.*, 2018, **44**, 10315.

92 W. Li and R. W. Schwartz, Ac conductivity relaxation processes in $CaCu_3Ti_4O_{12}$ ceramics: grain boundary and domain boundary effects, *Appl. Phys. Lett.*, 2006, **89**, 242906.

93 P. Bruce, High and low frequency Jonscher behavior of an ionically conducting glass, *Solid State Ionics*, 1985, **15**, 247.

94 D. Panda, S. S. Hota and R. N. P. Choudhary, Development of Lead-Free Defect Brownmillerite Perovskite Ceramic $LiBiFeMnO_5$ Solid Solution for Electronic Devices, *Adv. Eng. Mater.*, 2024, **26**, 2400010.

95 D. Panda, S. S. Hota and R. N. P. Choudhary, Structural, morphological, dielectric, and electrical characteristics of a brownmillerite material for electronic devices: $KBiMn_2O_5$, *Chem. Phys. Impact*, 2024, **8**, 100540.

96 D. Panda, S. S. Hota and R. N. P. Choudhary, Development of a complex strontium bismuth molybdate material: microstructural, electrical, and leakage current characteristics for storage and electronic device application, *Mater. Res. Bull.*, 2024, **174**, 112727.

97 K. Lee, S. Cho, S. H. Park, Z. J. Heeger, C.-W. Lee and S.-H. Lee, Metallic transport in polyaniline, *Nature*, 2006, **441**, 65.